# Guidance and Control for a Mars Helicopter

Håvard Fjær Grip[★,*], Daniel P. Scharf[★,†], Carlos Malpica[★★,‡], Wayne Johnson[★★,§],
Milan Mandić[★,¶], Gurkirpal Singh[★,‖], and Larry Young[★★,**]

[★]*Jet Propulsion Laboratory, California Institute of Technology, Pasadena, CA 91109*
[★★]*NASA Ames Research Center, Moffet Field, CA 94035*

**As part of a future mission to Mars, NASA is considering including a small helicopter capable of operating independently in the Martian environment. The Martian atmosphere is extremely thin, with a density of only 1–2% of Earth's atmospheric density at sea level; this significantly alters the flight dynamics of the vehicle and has implications for vehicle design and control. In this paper we focus on guidance and control for a Mars Helicopter, and in particular on the challenges that are unique to operating in the Mars environment. In 2016, the first-ever controlled flight of a helicopter in Martian atmospheric conditions was performed in the 25-ft Space Simulator at NASA's Jet Propulsion Laboratory. We provide details of the effort leading to this flight demonstration, including modeling, simulation, system identification, guidance, and control.**

## I. Introduction

From the first successful flyby by *Mariner 4* in 1964, human exploration of Mars has evolved via the use of orbiters and stationary landers, to the current use of wheeled rovers to unlock the secrets of the Red Planet. The most recent of NASA's Mars rovers is the car-sized *Curiosity*, which has been operating on the Martian surface since 2012.

As part of a future mission, NASA is considering sending a small helicopter to the Martian surface. The helicopter would be deployed after landing and would operate independently thereafter. Its purpose would be to perform a *technology demonstration*, verifying the feasibility of using helicopters for future Mars exploration by executing a series of fully autonomous flights.

The use of helicopters promises to bridge a gap in current Mars exploration capabilities. Orbiters have provided high-altitude aerial imagery of Mars, but with limited resolution. Rovers provide rich and detailed imagery of the Martian surface, but move at a slow pace and are limited by traversability of the terrain and line-of-sight. Helicopters, on the other hand, can quickly traverse large distances without being hindered by terrain, while providing detailed imagery of the surface from heights of a few meters to tens of meters above the surface. Paired with a rover, a helicopter can act as a scouting platform, helping to identify promising science targets or mapping the terrain ahead of the rover. Looking further ahead, helicopters may one day carry their own science payloads to areas that are inaccessible to rovers.



Fig. 1    Artist's concept of the proposed Mars Helicopter

### A. Challenges of Mars Helicopter Flight

Like any spacecraft or spacecraft instrument, a helicopter designed for Mars faces a host of challenging requirements not typically seen on Earth: it must withstand high structural loads during launch, extreme temperature variations, high

---

*Mars Helicopter GNC and Aerodynamics Lead, Robotics Technologist, JPL Guidance and Control Section; Havard.F.Grip@jpl.nasa.gov

†Senior Engineer, JPL Spacecraft Guidance and Control Group; Daniel.P.Scharf@jpl.nasa.gov; AIAA Senior Member

‡Aerospace Engineer, NASA Ames Aeromechanics Office; carlos.a.malpica@nasa.gov; AIAA Member

§Aerospace Engineer, NASA Ames Aeromechanics Office; wayne.johnson@nasa.gov; AIAA Fellow

¶Guidance and Control Engineer, JPL Guidance and Control Section; Milan.Mandic@jpl.nasa.gov

‖Guidance and Control Engineer, JPL Guidance and Control Section; gurkirpal.singh@jpl.nasa.gov

**Aerospace Engineer, NASA Ames Aeromechanics Office; larry.a.young@nasa.gov; AIAA Associate Fellow

levels of radiation, and be vacuum compatible; it must satisfy cleanliness requirements related to planetary protection; and it must operate entirely without physical intervention after launch. It must also be compactly designed to be carried as a spacecraft payload, and must be safely deployable after landing.

Design of a Mars Helicopter also faces distinct challenges in terms of the flight dynamics in the Martian environment. Two aspects of the environment are primary drivers for Mars helicopter flight dynamics:

- *Atmosphere*: the Martian atmosphere consists primarily of $CO_2$, and has a density of ***only 1-2% of Earth's atmospheric density*** at sea level, equivalent to altitudes of $100,000$ ft or more on Earth.
- *Gravity*: the Martian gravity is approximately 38% of Earth's gravity.

Designing a helicopter for Mars also presents serious challenges in terms of testing, verification, and validation. It is not practically possible to fully replicate the Mars environment on Earth; this forces a greater reliance on analysis, modeling, and simulation than for a typical small-scale rotorcraft program on Earth, combined with limited testing in partially replicated environments.

## B. Controlled-Flight Demonstration Effort

To better understand the issues related to helicopter flight dynamics and controllability on Mars, an effort was undertaken to demonstrate the feasibility of controlled flight. This effort culminated in the successful demonstration of fully autonomous helicopter flight in the 25-ft Space Simulator at NASA's Jet Propulsion Laboratory (JPL) in May 2016—the first-ever helicopter flight in Martian atmospheric conditions. The flight was conducted with a custom-designed co-axial demonstrator vehicle built by AeroVironment, Inc., the primary industry partner on the Mars Helicopter project (see Fig. 2). The vehicle featured a 1.21-m diameter rotor—the same size as intended for Mars flight. Because the vehicle had to lift its own weight on Earth, it did not carry batteries or an avionics computing platform, but was instead connected to a ground station via power and data tethers hanging below the vehicle.

The flight demonstration was preceded by a period of intensive modeling and analysis of flight dynamics, which led to specific requirements on the vehicle design to ensure adequate controllability under Martian conditions. It is nonetheless the case that modeling alone is insufficient for robust flight control design, due to a high degree of modeling uncertainty and the almost complete lack of prior work on flight dynamics in Mars-like conditions. Consequently, a *system identification* program was developed to identify the actual dynamics of the vehicle as-built. This program was custom-designed to allow the system identification to take place in the confined environment of JPL's 25-ft Space Simulator.



**Fig. 2   In this image, the Mars Helicopter demonstration vehicle is taking off for the first controlled flight in Martian atmospheric conditions, inside JPL's 25-ft Space Simulator.**

## C. Topics of this Paper

In this paper we focus on the guidance and control of a Mars Helicopter, including the challenges specific to operating on Mars. We will cover the following topics:

- overview of the Mars Helicopter prototype vehicle, including actuators and onboard sensing
- overview of the guidance, navigation, and control (GNC) architecture
- Mars Helicopter flight dynamics, including differences with Earth helicopter flight dynamics
- Mars-specific vehicle requirements to ensure adequate controllability of the vehicle
- modeling of the vehicle, using a combination of existing and newly developed tools
- system identification of the helicopter dynamics
- design of robust controllers
- results from free-flight testing

We end with a discussion of the remaining work for a flight-ready Mars implementation.

2

### D. Previous Work on Mars Helicopter Technology

Concepts for employing aerial vehicles to explore Mars have been proposed since the earliest days of space exploration. However, only after the Viking Lander missions of the 1970s did the full challenges of flight in the extremely thin, cold, and primarily $CO_2$-based atmosphere of Mars become apparent. For approximately two decades afterwards only Mars airplane concepts were studied. One of the first papers to consider the design implications of Mars rotorcraft was by Savu and Trifu [1]; this work, however, was not carried forward beyond its initial study.

In 2000, Stanford University and JPL attempted a proof-of-concept test of a small rotor under Mars-like atmospheric conditions in a JPL vacuum chamber [2]. No experimental results were published from this initial proof-of-concept test, though video was released at the time. Independently, at approximately the same time, a series of papers were published by NASA Ames Research Center studying the technical challenges of various Mars rotorcraft configurations and other vertical lift planetary aerial vehicles [3–6].

In 2000, Sikorsky Aircraft and NASA Ames Research Center co-sponsored the AHS International Student Design Competition on the topic of a Mars rotorcraft. Thompson [7] and Datta et al. [8] summarized the respective contributions of the Georgia Tech and University of Maryland Mars rotorcraft design entries. In 2002, the first experimental results for a rotor hover test under Mars-like conditions was published [9]. Over the next decade-and-a-half, papers continued to be occasionally published by NASA Ames [10–14] on the topic of planetary aerial vehicles, both fixed-wing and vertical lift aerial vehicles. As time went on, papers by other authors, organizations, and countries began to be published on Mars rotorcraft and vertical lift planetary aerial vehicles [15, 16].

In 2014, NASA JPL and AeroVironment published an initial paper on what would ultimately become the conceptual foundation for the current Mars Helicopter effort [17]. The current design, described in a recent paper [18], has evolved significantly but retains many of the original core features.

Although several of the papers cited were concerned with feasibility of Mars rotorcraft from the point of view of thrust generation and power consumption, they did for the most part not address the flight dynamics or the design of closed-loop control for Mars rotorcraft. A recent paper by some of the authors [19] explores the flight dynamics of a Mars Helicopter in detail.

## II. The Mars Helicopter Vehicle

The current Mars Helicopter is a *co-axial* design, with two counter-rotating 2-bladed rotors of radius 0.605 m, spaced apart by approximately 17% of the rotor radius (see Fig. 3). The rotor is *hingeless*, meaning that the blades are rigidly mounted on the hub, and only flex due to structural elasticity.

Compared to an Earth helicopter, the rotor is significantly oversized relative to the rest of the helicopter. The gross vehicle weight is less than 1.8 kg, a substantial portion of which is taken up by the batteries. The batteries can support flights lasting up to 90 s, while also providing sufficient energy for non-flight operation of the onboard electronics and night-time survival heating. The batteries are rechargeable via a solar panel mounted on the non-rotating mast above the upper rotor. The batteries and other electronics are housed in a cube-like fuselage attached to the central mast, inside of which is a *warm electronics box* that is properly insulated and heated to protect against low night-time temperatures.
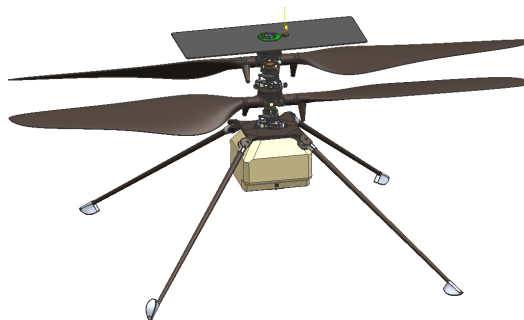


**Fig. 3   CAD drawing of the proposed Mars Helicopter**

### A. Actuation

During flight, the rotors operate at constant speeds of up to 2800 RPM, depending on the atmospheric density at the time of flight. The rotor RPM is not used to control the vehicle during flight; instead, the helicopter is controlled via *swashplates* on the upper and lower rotors. A swashplate is a mechanical device that permits the application of two types of control on the rotor:

- *Collective control* involves a change of the blade pitch on all the blades on a single rotor. When the blade pitch is increased, the angle-of-attack is increased, and the rotor produces more thrust. The Mars Helicopter has a 22°

collective control range on each rotor.

- *Cyclic control* involves a *periodic* change of the blade pitch on a single rotor—the blade pitch is increased on one side of the rotor disk, and decreased on the other side. The result is an asymmetric generation of lift, which gives rise to roll and pitch moments on the vehicle. Cyclic control is divided into two channels: *cosine cyclic* peaks at the rear of the rotor disk, whereas *sine cyclic* peaks on the right-hand side of the rotor disk. The Mars Helicopter has a ±10° cyclic control range on both rotors.

For a coaxial helicopter, use of the collective and cyclic control mechanisms can be summarized as follows:

- To control the helicopter in *heave* (translation along the vertical axis), collective is changed on both rotors, in the same direction. This form of actuation, referred to as *symmetric collective*, changes the overall thrust produced by the rotors.
- To control the helicopter in *yaw* (rotation about the vertical axis), collective is changed on both rotors, but in opposite directions. This form of actuation is known as *antisymmetric* or *differential collective*; it has the effect of leaving the overall thrust approximately the same while changing the drag on each rotor, thus imparting a net yaw moment on the vehicle.
- To control the helicopter in *roll and pitch*, cyclic control is used to generate asymmetric lift over the rotor disk.
- The *horizontal translation* of the helicopter is controlled indirectly via roll and pitch. When the vehicle attitude is changed, a portion of the thrust vector is in the horizontal plane, thereby accelerating the vehicle horizontally.

The above description is simplified, in the sense that each control is precisely associated with a response in a particular axis. In reality there are couplings between the axes that have to be accounted for in the control design.

### B. Navigation Sensors

Onboard navigation is performed using a combination of a small, MEMS-based inertial measurement unit (IMU), a low-resolution downward-looking camera, and a laser rangefinder. The IMU, which measures accelerations and angular rates, is used for propagation of the vehicle state from one time step to the next. The camera is used together with the laser rangefinder to determine the height above ground and the translational velocity; this information is fused with the IMU solution to limit drift over time. Details of the navigation design will be published in a future paper.

### C. Demonstration Vehicle

The vehicle used to demonstrate controlled flight in JPL's 25-ft Space Simulator is shown in Fig. 4. It features a full-scale rotor similar to the intended Mars vehicle. However, since this vehicle was required to lift its own weight in Earth gravity, anything non-essential to the demonstration of controlled flight was left off the vehicle to reduce weight. Instead of onboard batteries, power was provided through an electrical tether hanging below the vehicle.

Unlike the Mars vehicle, the flight demonstration vehicle was only equipped with cyclic control on the lower rotor. This provides sufficient degrees of freedom to control the helicopter as outlined in Section II–A, but results in greater cross-axis coupling due to asymmetry between the rotors.

For the demonstration vehicle, navigation was performed using a *Vicon* motion capture system, which determines both the position and attitude of the vehicle by tracking IR retroreflective targets on the vehicle using cameras positioned around the perimeter of the vacuum chamber. To compensate for latency in the Vicon measurements and to ensure robustness against potential outages, the Vicon solution was fused with data from an onboard IMU in an Extended Kalman Filter (EKF). The navigation algorithm and all other flight control functionality was hosted on a ground computer, which received IMU data
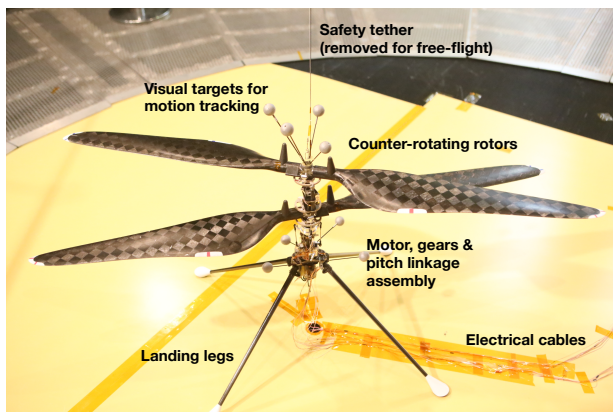


**Fig. 4 The vehicle used for controlled-flight demonstration in Martian atmospheric conditions was custom-built by AeroVironment, Inc.**

from the vehicle and transmitted actuator commands back to the vehicle via a data tether hanging below.

## III. Requirements and Operating Conditions

The Mars Helicopter is being designed for a *technology demonstration*, intended to show the feasibility of using helicopters for Mars exploration. The main GNC requirement is to safely perform several autonomous end-to-end flights, and as such, GNC performance requirements are driven by what is required to keep the vehicle safe.

The vehicle is designed to operate in densities between approximately 0.014 and 0.02 kg/m$^3$. In this density range, the vehicle is designed to have the power and aerodynamic capability to achieve thrust levels of at least 40% above hover thrust before the onset of stall. The vehicle will take off and land in an area that has already been inspected and is known to have acceptable limits on ground slopes. The helicopter will only fly in favorable weather conditions, with wind velocities limited to 9 m/s horizontally and 2 m/s vertically, with a maximum gust component of 3.5 m/s. Based on the forecasted weather, ground speed and climb/descent speeds will be limited such that maximum airspeed does not exceed 10 m/s horizontally and 3 m/s vertically.

When flying in an enclosed volume like JPL's 25-ft Space Simulator, downwash from the helicopter rotor is recirculated and results in gusts on the vehicle. The magnitude of these is hard to predict *a priori*; for the risk reduction phase, a gust corresponding to a 5 m/s step in airspeed was considered as the bounding scenario.

When designing controllers for the vehicle, two driving requirements emerge from the above considerations:
- maintain adequate stability margins over the entire flight envelope
- limit horizontal excursions due to gust, to avoid tipover on landing and collision (when flying in an enclosed volume)

## IV. Guidance and Control Architecture

Figure 5 illustrates the high-level architecture of the guidance, navigation, and control subsystem. Based on commands from a ground station, the *Mode Commander* is responsible for setting the mode of the other software modules according to the current phase of flight, as well as initiating any actions associated with transitions between modes (e.g., planning of a new trajectory). The *Navigation* module uses sensor data to estimate the state of the vehicle, which is used by the *Control* module, and intermittently by the *Guidance* module and the Mode Commander. The Guidance module produces reference trajectories and feedforward control signals based on the current phase of flight. The control module adds feedback control based on the difference between the reference trajectories and the estimated state, which yields the actuator commands.
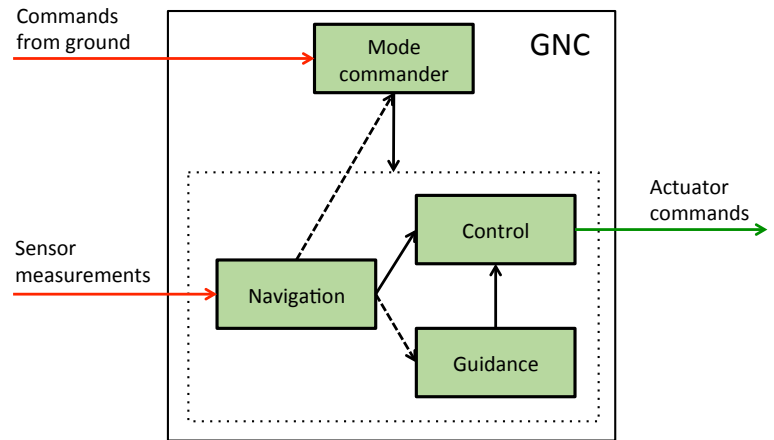


**Fig. 5 High-level GNC architecture. Red arrows illustrate information flowing into the system; green arrows illustrate information flowing out of the system; solid black arrows illustrate continuous information flow within the GNC system; dashed black arrows illustrate intermittent information flow within the GNC system.**

### A. Mode Commander

The mode commander is implemented as a state machine, which for the controlled flight demonstration described in Section I–B is illustrated in Fig. 6. The modes are as follows:
- *Idle*: await command from ground station
- *Estimator initialization*: wait for convergence of navigation solution as indicated by estimated error covariance matrix
- *Spinup*: rotor spinup to flight RPM
- *Takeoff preparation*: temporary open-loop application of nonzero thrust below takeoff thrust, to reduce magnitude of motor load increase on takeoff
- *Takeoff*: open-loop application of thrust to quickly climb a few centimeters away from ground. During this phase, only attitude *rates* are controlled, to minimize potential for destructive interaction with the ground while controller

5

is active.
- *Climb*: climb to hover altitude while translating to target horizontal position
- *Hover*: station-keep at target horizontal and vertical position
- *Descent*: descend while station-keeping at target horizontal position
- *Landing*: at an altitude of a few centimeters above ground, reduce thrust to settle on the ground with no closed-loop control, to prevent interaction with ground while controller is active.
- *Spindown*: Spin down to zero RPM

Flights can be aborted if a fault is detected, or by command from the ground station, as indicated by the red arrows in Fig. 6. For Mars flight, the mode commander is similar, except that the helicopter will track waypoints rather than executing a simple hover.
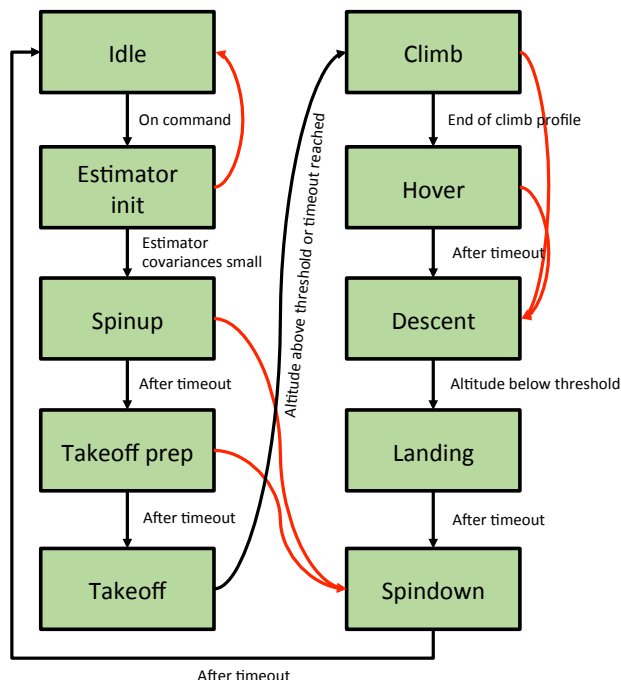


**Fig. 6   Mode commander states and transitions for controlled-flight demonstration. Red lines illustrate transitions triggered due to a detected fault or an abort command from ground.**

## B. Guidance

The guidance algorithms are responsible for generating reference trajectories for the helicopter to follow, as well as feedforward signals for the control inputs. Guidance is based on a simplified reference model that treats the helicopter as a thrust vector that can be tilted to produce horizontal accelerations. Differences between the reference model and the actual system, as well as any environmental disturbances, are handled via feedback.

For each of the translational channels, the guidance is based on an algorithm that plans consistent trajectories in position, velocity, acceleration, and jerk, while respecting adjustable limits on the maximum velocity, acceleration and jerk. The algorithm is designed to keep transition times small by generating trajectories that are always at one of the limits.

For heave, the position and velocity trajectories are used directly, while the acceleration trajectory is converted to an equivalent control feedforward via model parameters. For horizontal translation, the position and velocity trajectories are used directly; the acceleration trajectory is converted to equivalent roll and pitch angles, and the jerk trajectory is converted to equivalent roll and pitch rates. Feedforward control inputs are in this case set to zero.

For yaw, the same planning algorithm is used to produce consistent trajectories in yaw angle, yaw rate, yaw acceleration, and jerk. Yaw angle and yaw rate are used directly, while yaw acceleration is converted to control

6

feedforward. In addition, the yaw guidance contains provisions for selecting the shortest rotation toward the target heading and protection against yaw angle wrapping.

## C. Control

Figure 7 illustrates the overall control architecture during flight, which mirrors typical helicopter control architectures used elsewhere (see, e.g., [20] and references therein).

Heave is controlled by a PID-type controller feeding back estimated vertical position provided by the navigation subsystem. Yaw angle is similarly controlled by a PID-type controller. The horizontal position of the vehicle is controlled via a nested architecture. An inner loop is formed by independently controlling roll and pitch with PD-type controllers. Input to the inner loop is set by an outer loop, which is formed by controlling the horizontal position using PID-type controllers. The horizontal position is represented in a local ground frame, whereas the roll and pitch angles are the angles of the body frame relative to gravity; therefore, the output of the outer loop is rotated by the yaw angle before being used as a reference by the inner loop.

The green arrows in Fig. 7 illustrate the guidance reference trajectories and control feedforward signals. Not shown in Fig. 7 is the fact that derivative action in each control loop is implemented not by numerically differentiating the input, but by combining estimates of the derivatives, as provided by the navigation module, and the derivatives of the reference trajectories, as provided by the guidance module; this improves the response by eliminating the noise amplification inherent in numerical differentiation.
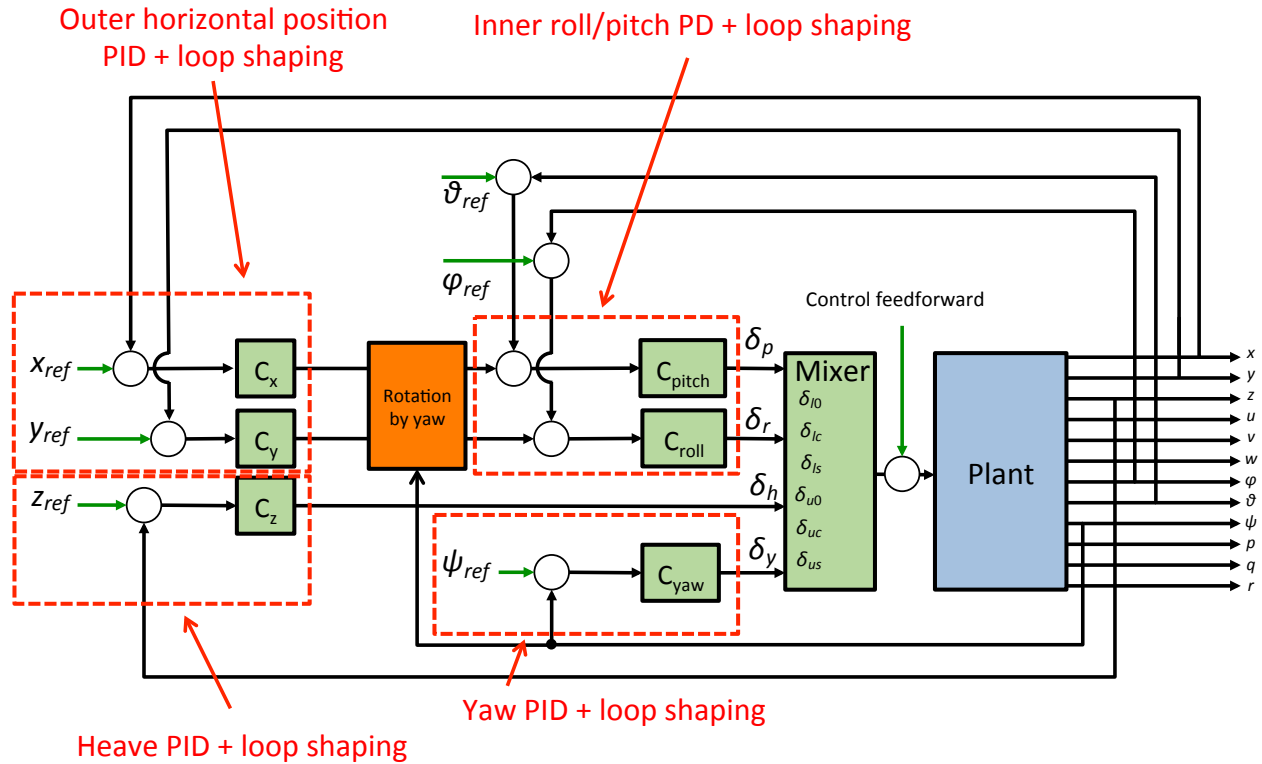


**Fig. 7 Overall control architecture. Positions in the ground frame are denoted by $[x; y; z]$; velocities in the body frame are denoted by $[u; v; w]$; Euler angles and angular rates with respect to the ground frame are denoted by $[\phi; \theta; \psi]$ and $[p; q; r]$. Commanded lower collective, lower cosine cyclic, and lower sine cyclic are denoted by $[\delta_{l0}; \delta_{lc}; \delta_{ls}]$; similar for the upper controls. The symbols $\delta_r$, $\delta_p$, $\delta_h$, and $\delta_y$ denote linear combinations of the control inputs to produce inputs aligned with the roll, pitch, heave, and yaw axes.**

7

Although each control loop is built around a PD or PID controller, this turns out to be insufficient by itself to achieve satisfactory stability margins for the Mars Helicopter. Higher-order loop shaping is therefore used to improve the margins without significantly sacrificing performance, as shown in Section IX.

A static mixer is used in Fig. 7 to align the control inputs with the axes being controlled. It is nevertheless the case that couplings exist between the various axes. Final determination of stability margins is therefore done using multiple-input multiple-output (MIMO) tools, as discussed in Section IX.

Because the dynamics of a helicopter changes depending on the flight regime, it is common to gain schedule the controller based on airspeed. However, no airspeed measurement is available on the Mars Helicopter, and within the operating envelope, the ground speed is far smaller than the maximum wind speeds that may be encountered, the direction of which is unknown. Therefore, virtually no information is available for gain scheduling, so a single set of gains must be designed for the whole envelope. Different sets of control gains may nevertheless be used depending on the *density* at the time of flight, which will be known to a close approximation.

## V. Mars Helicopter Flight Dynamics

The analysis of helicopter flight dynamics is considerably complicated by the fact that the airfoils are rotating rather than stationary relative to the body frame of the vehicle. Inputs to the vehicle, whether as a result of controls or environmental disturbances, therefore tend to produce *periodic* forces and moments, whose gross effect on the vehicle motion must be well understood in order to design robust control.

Consider the effect of a sine cyclic control input, peaking on the right-hand side of the vehicle. The result of such a control input is a periodic modulation of the lift, also peaking on the right-hand side of the vehicle. It is tempting to assume that this will produce a leftward roll moment. However, this is an incorrect assumption in general, and the actual response can only be understood by considering the dynamics of *rotor flapping*—i.e., the out-of-plane motion of the rotor blade, as illustrated in Fig. 8.

### A. Blade Flapping

To understand how blade flapping affects the helicopter flight dynamics, it is useful to start with the simplest possible model of the blade, as a rod rotating about a hinge point with a spring, as shown in Fig. 8. The spring force on the hinge is due to a combination of *centrifugal stiffening* and structural stiffness, whereas the damping is predominantly aerodynamic. Some rotors have actual hinges to enable flapping, but for hingeless rotors, such as the Mars Helicopter rotor, the hinge is a simplified model of the flexing due to elastic deformation of the blade.

When cyclic pitch is applied to a helicopter blade, a periodic change in lift is produced at the frequency of the rotor rotation, with maximum lift on one side of the rotor disk, and minimum lift on the opposite side. The blade responds like a mass-spring-damper subjected to a periodic force; meaning it will flap with the same frequency, but a different phase than the input.

The blue line in Fig. 9 shows an example magnitude and phase response of the blade flap angle in response to
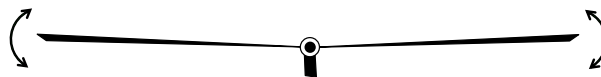


**Fig. 8    Illustration of blade flapping modeled by a central hinge. Depending on the rotor being modeled, a spring providing restoring moments may be associated with the hinge.**

blade pitch, for a centrally hinged rotor with typical Earth parameters. The red line represents the rotor speed—i.e., the frequency at which cyclic pitch modulation is applied. In this example, the rotor speed coincides with the natural frequency of the mass-spring-damper, meaning that the peak flap output will occur 90° *after the peak cyclic pitch input*. For this rotor, a cyclic input peaking on the right-hand side of the vehicle would therefore result in a nose-up moment on the vehicle. For stiffer rotor designs, the natural frequency will increase, resulting in a smaller phase angle, but for typical Earth helicopters it is still 45° or more.

The green line in Fig. 9 shows the same flap response in Mars density. The response is dramatically different because of reduced aerodynamic damping. It is clear that the phase angle is now extremely sensitive around the natural frequency, and will quickly drop to near-zero if the rotor is stiffened to increase the natural frequency.

The azimuthal phase angle of the flap response is easily compensated for in a controller by the appropriate static mixing of the two cyclic channels. More concerning from the point-of-view of control is the *transient* flap response. A poorly damped mass-spring-damper takes longer to converge to steady-state; ultimately this manifests itself as poorly damped modes in the attitude response of the helicopter as a whole.
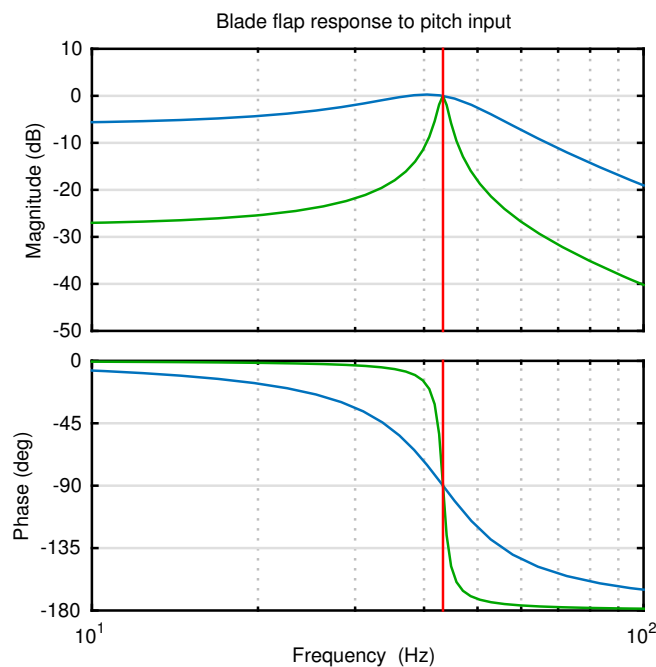
**Fig. 9   Magnitude and phase of blade flap angle response to pitch input, for a centrally hinged blade with no additional stiffness. Blue: typical Earth response. Green: hypothetical response in Mars atmosphere.**

### B. Effect of Flap Modes on the Helicopter Dynamics

The flap dynamics studied in the last section represents the motion of the blade when studied from the *rotating* frame—that is, what would be seen by an observer attached to the rotor hub and following along with the azimuthal rotation of the blade. When controlling the helicopter, we are instead interested in the overall dynamics as seen from the helicopter body frame. The resonant flap mode seen in Fig. 9 then gives rise to *two* modes, called the *regressing* and *advancing modes* (see [19] for more detail). A formal study of these modes can be conducted by a transformation into *coning* and *tip-path plane* coordinates (see, e.g., [21]). Such a study reveals that these modes inherit the low level of damping of the non-rotating flap mode. Figure 10 shows the magnitude of the transfer function from cosine cyclic (peaking at the rear of the rotor disk) to pitch angle, for a particular version of the Mars helicopter dynamics that was studied at an early point. The regressing and advancing flap modes clearly visible.

### C. Consequences of Flap Dynamics for Control and Vehicle Design

Poorly damped modes like the ones shown in Fig. 10 are problematic for control, due to the potential for destabilization through interaction with the control system. There are, broadly speaking, three main strategies available to deal with modes of this kind:

1) *phase-stabilizing* the modes, by ensuring that the phase of the control loop prevents unwanted encirclements of the critical point
2) employing *notch filters* to reduce the gain of the control loop at the particular frequencies in question
3) *gain-stabilizing* the modes by ensuring that the control loop gain rolls off well in advance of the modes

Of these, the first two require good knowledge of the dynamics around the relevant frequencies, and confidence that the dynamics will never change. Such assumptions are not well justified for the Mars Helicopter, in part because of the difficulty of accurately identifying dynamics at these frequencies in the right environment; and in part because the actual dynamics, once other sources of flexibility (e.g., bending of the mast) are coupled in with the flap dynamics, will look far more complicated than what is indicated in Fig. 10.

The third option is far more robust, but in general may place restrictions on achievable closed-loop bandwidth. For
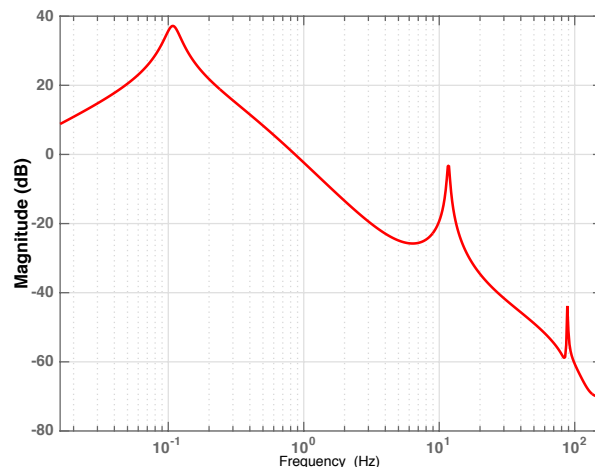
9

**Fig. 10   Magnitude of pitch angle frequency response to cosine cyclic input, for a particular version of the Mars Helicopter dynamics. The poorly damped regressing and advancing flap modes are clearly visible.**

the Mars Helicopter, there are minimum bandwidth requirements due to
  • the need to stabilize the helicopter dynamics, which is open-loop unstable (see Sections VII–A and IX–C)
  • performance requirements in gusty conditions
In order to achieve the necessary bandwidth, the resonant modes must instead be moved to sufficiently high frequencies through the mechanical design. To the achieve this, the blades and hub for the Mars Helicopter are designed to be unusually stiff, with a rotating flap frequency of approximately 80–90 Hz. Together with other stiffness requirements for the mast and landing gear, all resonant modes in the flight dynamics are then moved to sufficiently high frequencies.

### D. Gust Sensitivity and Drawbacks of Stiff Rotor Design

A helicopter generates thrust by imparting moment to the surrounding air, like a fan. This results in airflow through the rotor, called *inflow*, which for the Mars Helicopter has a magnitude of approximately 10 m/s. When the helicopter is hovering, the inflow is relatively uniform across the rotor disk. However, if the helicopter moves horizontally relative to the air, an inflow gradient is generated over the rotor disk, resulting in more inflow at the rear of the rotor disk, and less at the front. The result of this gradient is to reduce the lift at the rear of the disk and to increase it at the front, which gives rise to a pitch moment away from the wind. This in turn causes the vehicle to translate, due to the tilt of the thrust vector.

The high stiffness of the rotor increases the sensitivity of the helicopter response to gusts through several mechanisms, as described in [19]. This is a drawback of the stiff rotor design, which also affects open-loop stability, as discussed in Section VII–A. On the other hand, the reduced gravity on Mars helps to mitigate the translational sensitivity to gust (see [19]).

## VI. Modeling and Simulation

Simplified analysis is useful for understanding the basic drivers of the helicopter flight dynamics, and how these are affected by the Mars environment. To capture the dynamics with higher levels of fidelity, however, nonlinear modeling and simulation tools are needed. The primary tool for studying flight dynamics for the Mars Helicopter is called *Helicopter Control Analysis Tool* (*HeliCAT*). It was developed specifically for this purpose, using the *Darts/Dshell* multibody simulation framework developed at JPL (see, e.g., [22]). It models the helicopter as a collection of rigid bodies, which are connected by hinges with springs and dampers to represent flexibility. The aerodynamics is based around airfoil tables obtained from CFD, augmented with additional effects representing radial drag, tip losses, and unsteady aerodynamics (see [23]). Inflow is modeled based on the nonlinear dynamic inflow model of Peters and HaQuang [24], which represents the inflow as a uniform component plus a linear gradient over the rotor disk. Validation and additional high-fidelity studies are performed using CAMRAD II, a comprehensive analysis tool for rotorcraft that is widely used across NASA and in industry.

10

The strength of HeliCAT is in the features tailored toward GNC design, including:

- detailed modeling of actuators and sensors, including camera imaging
- modeling of ground contact dynamics, including varied terrain and terrain properties
- modeling of ground support equipment, such as gimbals and force-torque sensors, for validation of the system identification approach
- flight software integration
- 3D visualization

In addition to generating models for control analysis, HeliCAT can be used to execute simulations of end-to-end missions with flight software in the loop. Figure 11 shows a snapshot of simulated Mars flight within Victoria crater on Mars. Additional information on the modeling approach can be found in [19].



**Fig. 11 HeliCAT visualization of the helicopter flying on Mars, with flight software in the loop.**

### A. Obtaining Linear Models for Control Design

For control analysis and design, it is desirable to obtain linear time-invariant (LTI) models of the flight dynamics, as this enables the use of a wide variety of frequency-domain design and analysis tools. For a typical plant, this is done by linearizing the nonlinear dynamics about an equilibrium point.

For a helicopter, this is more challenging, due to the periodic nature of the dynamics. Even in steady-state flight, the helicopter is undergoing periodic motion—the blade pitch varies periodically due to cyclic control, the blades flap due to periodic lift changes from control and the environment, the fuselage vibrates due to reaction forces, etc. Thus, the equilibrium is not constant, but is instead characterized by a periodic trajectory, with fundamental frequency corresponding to the frequency of the rotor rotation. For a specified steady-state velocity, HeliCAT computes the corresponding equilibrium trajectory by solving a numerical problem based on the difference in the multibody state before and after a single revolution of the rotor; for hover flight, this difference should be zero.

Once a periodic equilibrium trajectory has been identified, the multibody model can be linearized about any point along the trajectory. Each linearization will yield a different system. It is common to perform linearizations at a finite set of uniformly spaced points along the trajectory, which yields a periodic linear time-varying system. From
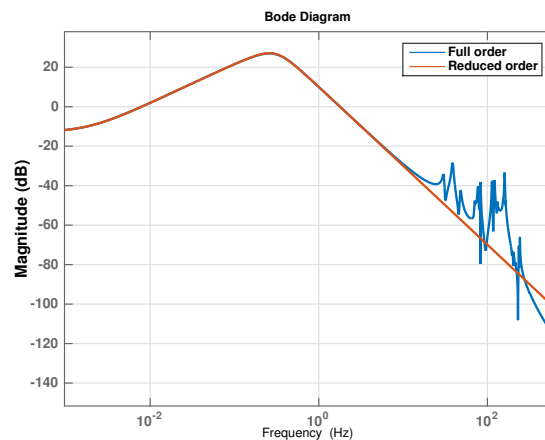


**Fig. 12 Comparison of the full-order and reduced-order linear models, for an up-to-date model of the Mars Helicopter. The complicated dynamics at high frequency is a result of poorly damped rotor dynamics, combined with flexibility of the mast and the landing gear.**

this periodic system, one could obtain an LTI model through simple averaging; however, this method yields an inaccurate response for the Mars Helicopter, due to the time-varying coupling between the rotor and fuselage with two-bladed rotors.

We instead post-process periodic linear time-variant models generated by HeliCAT using a method similar to Lopez and Prasad [25]. The method extends the vehicle state by including the coefficients of a truncated harmonic expansion: $x = x_0 + \sum_{i=1}^{n} (x_{ic} \cos(i\Omega t) + x_{is} \sin(i\Omega t))$, where $\Omega$ is the rotor angular rate. The resulting model is of high order, but captures the frequency response of the helicopter model with good accuracy, when compared to frequency sweeps of the nonlinear model. The high-order model can be reduced to a lower-order model on the form described in the

11

next section through a custom process that matches the pairwise frequency responses between plant input and outputs. Figure 12 shows the magnitude of the full-order and reduced-order frequency response of the transfer function from cosine cyclic input to the helicopter pitch angle, for an up-to-date model of the Mars Helicopter in hover. The low-order model matches the high-order model well up to frequencies of approximately 10 Hz, which is adequate for relying on the low-order formulation for control analysis and design. For more information on the linearization and model reduction process, see [19].

## VII. Low-Frequency Dynamics

The ability to represent the low-frequency dynamics with a low-order model is one of the benefits of a stiff rotor design. We use a model with only velocities, attitude, and angular rates as states, which can be written as

$$\dot{x} = Ax + Bu, \tag{1}$$

where $x = [u; v; w; \phi; \theta; \psi; p; q; r]$ contains the body-frame velocities relative to an inertial wind frame, the attitude Euler angles, and the body-frame angular rates; and $u = [\theta_{l0}; \theta_{lc}; \theta_{ls}; \theta_{u0}; \theta_{uc}; \theta_{us}]$ contains the lower collective, cosine cyclic, and sine cyclic, followed by the upper collective, cosine cyclic, and sine cyclic. We use the convention that the $x$ axis points forward on the vehicle; the $y$ axis points to the right; and the $z$ axis points down.

The $A$ and $B$ matrices are written in standard form as

$$A = \begin{bmatrix} X_u & X_v & X_w & 0 & -g\cos(\bar{\theta}) & 0 & X_p & X_q - \bar{w} & X_r + \bar{v} \\ Y_u & Y_v & Y_w & g\cos(\bar{\phi})\cos(\bar{\theta}) & -g\sin(\bar{\phi})\sin(\bar{\theta}) & 0 & Y_p + \bar{w} & Y_q & Y_r - \bar{u} \\ Z_u & Z_v & Z_w & -g\sin(\bar{\phi})\cos(\bar{\theta}) & -g\cos(\bar{\phi})\sin(\bar{\theta}) & 0 & Z_p - \bar{v} & Z_q + \bar{u} & Z_r \\ 0 & 0 & 0 & 0 & 0 & 0 & 1 & \sin(\bar{\phi})\tan(\bar{\theta}) & \cos(\bar{\phi})\tan(\bar{\theta}) \\ 0 & 0 & 0 & 0 & 0 & 0 & 0 & \cos(\bar{\phi}) & -\sin(\bar{\phi}) \\ 0 & 0 & 0 & 0 & 0 & 0 & 0 & \sin(\bar{\phi})/\cos(\bar{\theta}) & \cos(\bar{\phi})/\cos(\bar{\theta}) \\ L_u & L_v & L_w & 0 & 0 & 0 & L_p & L_q & L_r \\ M_u & M_v & M_w & 0 & 0 & 0 & M_p & M_q & M_r \\ N_u & N_v & N_w & 0 & 0 & 0 & N_p & N_q & N_r \end{bmatrix},$$

$$B = \begin{bmatrix} X_{L0} & X_{LC} & X_{LS} & X_{U0} & X_{UC} & X_{US} \\ Y_{L0} & Y_{LC} & Y_{LS} & Y_{U0} & Y_{UC} & Y_{US} \\ Z_{L0} & Z_{LC} & Z_{LS} & Z_{U0} & Z_{UC} & Z_{US} \\ 0 & 0 & 0 & 0 & 0 & 0 \\ 0 & 0 & 0 & 0 & 0 & 0 \\ 0 & 0 & 0 & 0 & 0 & 0 \\ L_{L0} & L_{LC} & L_{LS} & L_{U0} & L_{UC} & L_{US} \\ M_{L0} & M_{LC} & M_{LS} & M_{U0} & M_{UC} & M_{US} \\ N_{L0} & N_{LC} & N_{LS} & N_{U0} & N_{UC} & N_{US} \end{bmatrix}.$$

We have denoted by $[\bar{u}; \bar{v}; \bar{w}]$ the body-frame trim velocities; by $\bar{\phi}$ and $\bar{\theta}$ the trim roll and pitch attitudes; and by $g$ the acceleration of gravity. The remaining components of $A$ and $B$ are referred to as *stability derivatives* and *control derivatives*, and capture sensitivities of the vehicle motion to the states and control inputs.

### A. Open-Loop Stability

Unlike most vehicles, helicopters are almost always unstable in open loop, with poles in the *open* right-half complex plane. The Mars Helicopter is no exception in this respect, as can be seen from Fig. 13, which shows the open-loop poles of the hover dynamics of the Mars Helicopter demonstration vehicle. The dynamics exhibit four stable subsidence modes in the open left-half complex plane; one marginally stable mode at the origin; and four unstable modes in the

open right-half complex plane. The mode at the origin is due to the yaw angle, which does not affect the dynamics in any way. The modes in the right-half complex plane are longitudinal and lateral *phugoid* modes that result from a coupling between the attitude and horizontal speed states.
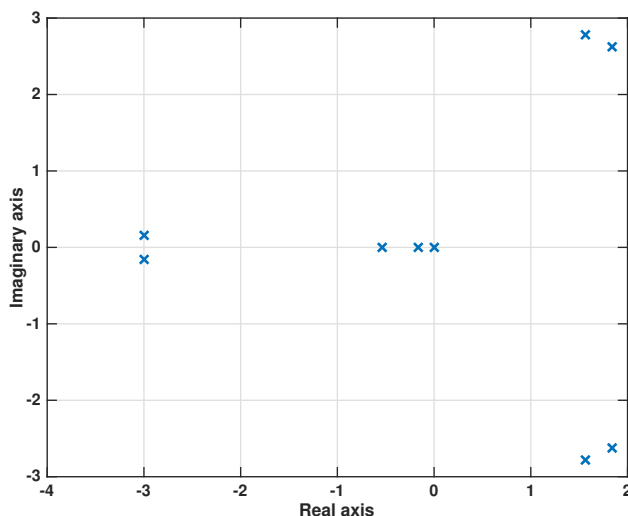


**Fig. 13    Poles of the low-frequency dynamics of the demonstration vehicle**

To see what drives these modes, consider the longitudinal dynamics only, restricted to the pitch angle, pitch rate, and longitudinal velocity. Assume furthermore that $X_u$ (longitudinal drag) and $M_q$ (pitch damping) are zero, which is close to the truth for the Mars Helicopter. At hover with zero trim angles, the resulting system matrix is given by

$$A_l = \begin{bmatrix} 0 & -g & 0 \\ 0 & 0 & 1 \\ M_u & 0 & 0 \end{bmatrix}.$$

The stability derivative $M_u$ represents the sensitivity of the helicopter's pitch rate to longitudinal speed; or equivalently, the sensitivity to a gust from the front. It is positive, because increased longitudinal velocity results in a nose-up moment.

The characteristic equation of $A_l$ is given by $\lambda^3 + M_u g = 0$, with solutions $\lambda_1 = -\sqrt[3]{M_u g}$, $\lambda_{2,3} = \frac{1}{2}(1 \pm \sqrt{3}j)\sqrt[3]{M_u g}$. It is clear that the frequency of the unstable poles increases with both $M_u$ and $g$. We can therefore make the following observations:

- As discussed in Section V–D, the high rotor stiffness results in increased gust sensitivity, which manifests itself as an increase in the magnitude of $M_u$. This results in an increase in the frequency of the unstable modes.
- The unstable modes for a helicopter operating in Mars gravity will have reduced frequency compared to Earth. In particular, the unstable modes shown in Fig. 13 for the demonstration vehicle will slow down for the same helicopter on Mars.

The unstable nature of the open-loop dynamics is highly significant in the context of control design, as it imposes fundamental limitations on the achievable stability margins by effectively placing a lower bound on the control gains (see Section IX–C). This limitation becomes more severe as the frequency of the instability increases. An excellent investigation of these limitations based on Bode integrals can be found in Stein [26].

As the helicopter moves from hover into forward flight, the longitudinal instability tends to increase in frequency (see [19]). The details and consequences of this will be treated in a future paper.

## VIII. System Identification

In spite of the extensive modeling and simulation effort, testing is needed to fully understand the vehicle behavior, especially given the lack of prior work on helicopter dynamics in Martian conditions. A system identification program has therefore been developed to identify the actual dynamics of the helicopter.

A unique challenge in performing system identification on the Mars Helicopter is the highly confined volume available for testing, which effectively prevents the gathering of free-flight data for the purpose of system identification. A "piecewise" approach is therefore adopted, in which individual parameters relevant to the dynamics are targeted through specific experiments that can be performed in a confined space. This approach is enabled by the stiff rotor design, which reduces the dynamics in the relevant frequency range to the well-defined, low-order system (1), which has relatively few parameters.

Here, we provide a summary of the approach to system identification applied to the demonstration vehicle; we refer to [19] for further details.

### A. System Identification for Demonstration Vehicle

System identification on the demonstration vehicle was performed through a number of experiments in three main configurations:

1) *Locked-down configuration*: the vehicle was mounted on a force-torque sensor
2) *Swinging-arm configuration*: the vehicle was mounted on a force-torque sensor at the end of a swinging arm
3) *Gimbal configuration*: the vehicle was mounted on a gimbal providing roll and pitch degrees of freedom

In the first configuration, the vehicle was first trimmed for hover. The control inputs were then exercised and the resulting forces and moments measured. This allowed the control derivatives for the translational degrees of freedom, as well as the yaw degree of freedom, to be identified, by dividing measured force and moment sensitivities with the mass and yaw moment of inertia, respectively.



**Fig. 14   The helicopter in the swinging-arm configuration. The 3-m long arm was swung back and forth to generate airflow over the rotor.**

It also allowed identification of the relative magnitude of the control derivatives in roll and pitch; however, the absolute magnitude of those control derivatives could not yet be determined, due to a larger *apparent inertia* in roll and pitch that had to be identified in a later step. The increased apparent inertia is a phenomenon described in [19], and results from out-of-plane flexing of the two counter-rotating rotors.



**Fig. 15   The helicopter in the gimbal configuration. The helicopter was placed upside-down due to improved air recirculation properties within the chamber and to make it easier to restrain during spinup and spindown.**

In the second configuration, the vehicle was swung back and forth in order to generate edgewise flow over the rotor, and the resulting forces and moments were measured to determine the speed stability derivatives (see Fig. 14). The absolute magnitude of the roll and pitch speed stability derivatives could not yet be determined, since the apparent inertia was not known. The helicopter was also turned on its side, to generate flow perturbations through the rotor, thereby identifying the heave damping stability derivative.

In the third configuration, control inputs were applied to the vehicle on the gimbal, which allowed the roll and pitch damping derivatives to be identified (see Fig. 15). It also allowed the apparent inertia in roll and pitch to be identified, thus providing the missing piece of information necessary to determine the control derivatives and speed stability derivatives in roll and pitch.

14

**B. System Identification Findings**

The system identification approach outlined above was successful in determining the key parameters of the system. Many of the smaller parameters could not be reliably identified due to noise and aerodynamic disturbances; however, this was expected and is of little consequence because of limited impact on the dynamics.

Some significant differences with *a priori* modeling were identified, most of which were associated with inflow modeling. Two key discoveries with respect to control were the following:

- The on-axis moments generated due to edgewise flow (gusts), as captured by the speed stability derivatives $M_u$ and $L_v$, were significantly larger than expected. This is most likely due to the development of a larger inflow gradient than predicted by the inflow model of Peters and HaQuang [24]. By adding a tuning parameter to amplify the inflow gradient, the result can be reproduced in simulation. The increased sensitivity degrades the open-loop stability properties of the system (see discussion in Section VII–A).

- The on-axis roll/pitch damping derivatives $M_q$ and $L_p$ were found to be *positive*, meaning that roll and pitch rates are self-amplifying rather than damped. This is contrary to typical helicopter behavior. The likely cause is a dependence of the inflow gradients on the roll and pitch rates of the rotor disk, which is not included in [24] but can be found elsewhere (e.g., [23]). The inclusion of this effect typically changes the off-axis response to control inputs, but due to the peculiarities of the Mars Helicopter flapping dynamics (see Section V–A), it instead has the effect of removing the roll and pitch damping. This property of the Mars Helicopter also affects the open-loop stability negatively.

## IX. Control Design and Analysis

Control design for the vehicle is based on reduced-order models on the form (1), augmented with a servo actuator model and time delays. Here we will present details of the specific control design for the demonstration vehicle, based on the system identification experiments discussed in Section VIII. The servo actuator in this case is modeled as a second-order system, with a bandwidth of 12 Hz and 85% damping, corresponding to the measurements made during system identification.

The GNC loop was executed at a rate of 500 Hz, triggered by IMU measurements from the vehicle at the same rate. For continuous-time control design, one half of the sampling interval (i.e., 1 ms) must be added as a time delay, to account for the discrete-time implementation. Another 4 ms is added as an estimated upper bound on the latency due to communication delays to and from the vehicle, execution time of the GNC loop, and latency due to the servo actuators triggering at an independent, asynchronous rate. Furthermore, 2.9 ms delay is added in the gyro measurements, and 5.8 ms delay is added in the accelerometer measurements, due to linear phase lag from FIR anti-aliasing filters on the IMU. For the purpose of analysis, the sensor-specific delays are lumped with the controller in the loops consuming the relevant data (i.e., gyro delays in the attitude controllers and accelerometer delays in the translational controllers), and the remaining delays are lumped with the servo model.

**A. Control Design Approach**

We wish to leverage single-input single-output (SISO) tools for control design to the greatest extent possible, while at the same time taking care to maintain good stability properties in a MIMO context. The chosen approach can be summarized as follows:

1) select collective and cyclic mixing matrices to approximately decouple control inputs
2) design SISO controllers for each individual control loop
3) check MIMO stability using multiloop *disk margins*

In reality, the last two steps are iterative, as the MIMO stability analysis will often reveal that changes are necessary to the individual control loop designs.

The primary objectives of the control design are to ensure adequate gain and phase margins in the presence of model uncertainty, and to achieve sufficiently good station-keeping performance in response to horizontal gusts (maximum displacement of 2 m in response to a 5 m/s gust).

15

## B. Heave and Yaw Control

Control of heave and yaw starts with the selection of a collective mixing matrix $M_{\text{col}}$, such that the product

$$\begin{bmatrix} Z_{L0} & Z_{U0} \\ N_{L0} & N_{U0} \end{bmatrix} M_{\text{col}} \tag{2}$$

is diagonal. By defining a yaw-aligned input $\theta_h$ and a heave-aligned input $\theta_y$ such that

$$\begin{bmatrix} \theta_{l0} \\ \theta_{u0} \end{bmatrix} = M_{\text{col}} \begin{bmatrix} \theta_h \\ \theta_y \end{bmatrix}, \tag{3}$$

we obtain heave and yaw dynamics that are decoupled from each other and—due to the values of other stability and control derivatives in hover—the rest of the system. Both the heave and yaw dynamics are now represented by second-order systems with additional actuator dynamics, for which PID-type controllers can be designed with relative ease. For the heave loop, a controller with crossover frequency of 1.2 Hz was designed, with stability margins of 15.5 dB and 60 deg. For the yaw loop, a controller with crossover frequency of 1.9 Hz was designed, with stability margins of 10.2 dB and 58 deg. Nichols charts for the heave and yaw loops are seen in Figs. 16 and 17. For the yaw loop, the loop has been shaped to "square out" the magnitude-vs-phase curve as it rounds the critical point, using a technique known as a *Bode step* [27]; this is done in order to improve stability margins without lowering the bandwidth.
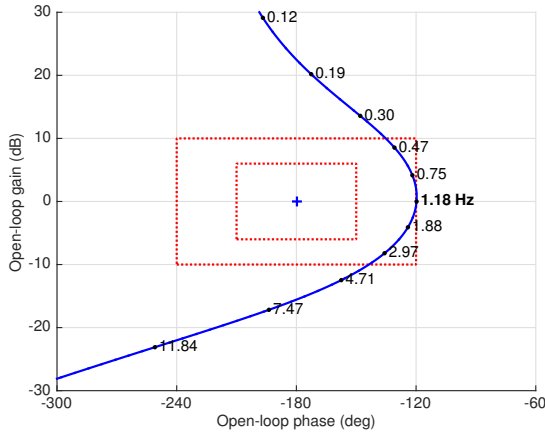


Fig. 16 Nichols chart for the heave loop. The inner red box indicates margins of 6 dB and 30°. The outer red box indicates margins of 10 dB and 60°.
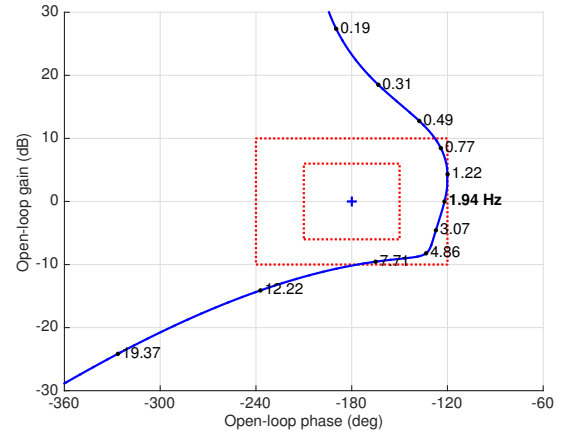
Fig. 17 Nichols chart for the yaw loop

## C. Roll, Pitch, and Horizontal Translation Control

Together, the roll, pitch, and horizontal translation dynamics form a coupled system, which will be controlled using a nested control design. The first step in the process is to construct a cyclic mixing matrix $M_{\text{cyc}}$, such that

$$\begin{bmatrix} L_{LC} & L_{LS} \\ M_{LC} & M_{LS} \end{bmatrix} M_{\text{cyc}} \tag{4}$$

is diagonal (recall that the demonstration vehicle only has cyclic control on the lower rotor, so we do not have upper cyclic channels). We then define a roll-aligned input $\theta_r$ and a pitch-aligned input $\theta_p$ such that

$$\begin{bmatrix} \theta_{lc} \\ \theta_{ls} \end{bmatrix} = M_{\text{cyc}} \begin{bmatrix} \theta_r \\ \theta_p \end{bmatrix}. \tag{5}$$

16

Application of the new inputs will result in pure roll and pitch moments according to the model, although coupling still exists due to the stability derivatives and the translational control derivatives.

Next, we design the inner and outer loops. The inner loop is designed by eliminating the translational degrees of freedom and designing for the system restricted to roll and pitch. A Nichols chart for the pitch control loop is shown in Fig. 18. The inner loop has a crossover frequency of 2.6 Hz and exhibits margins of 9.3 dB and 60 deg. The outer loop is designed by closing the inner loop and treating the negative pitch angle as the control input for longitudinal translational control and the roll angle as the control input for lateral translational control. A Nichols chart for the longitudinal translational loop is shown in Fig. 19. The outer loop has a crossover frequency of 0.3 Hz, with margins of 15.6 dB and 56 deg.
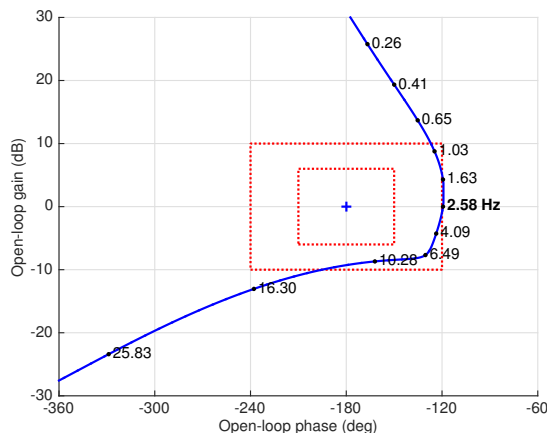


**Fig. 18    Nichols chart for the inner pitch loop**
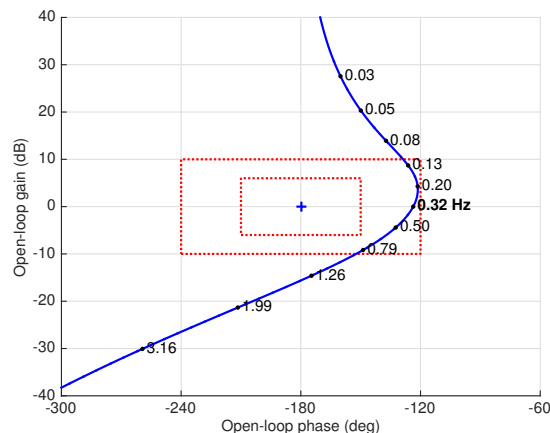


**Fig. 19    Nichols chart for the outer longitudinal translation loop**

Ideally, the sequential design process outlined above would be adequate for designing the nested controller. However, it is possible to design a controller with good stability margins both for the inner loop (with translational dynamics eliminated) and the outer loop (with the inner loop closed) that nevertheless reveals *inadequate* margins when the loop is opened up at the input point with *both* controllers in place, as illustrated in Fig. 20. Figure 21 shows the Nichols chart for the pitch/longitudinal translation axis when opened at this point. Properly shaping this curve, to achieve SISO margins of 9.3 dB and 60 deg, was only achieved through multiple iterations of the inner and outer loop design, and only by carefully shaping the inner loop to square out the curve as it rounds the critical point.

The loop shape in Fig. 21 is informative because it clearly reveals the limitations imposed by the open-loop instability. The curve of the magnitude-vs-phase plot passes both *above and below* the critical point, which means that both an increase and a reduction in gain will reduce the gain margin and eventually destabilize the system. Thus, whereas in most control systems the gain margin can be increased by lowering the gains (at the cost of decreased performance), such a trade is not possible for the helicopter.



**Fig. 20    Stability is studied by opening the plant at the input point, while leaving the roll/pitch and horizontal translation controllers in place.**

### D. MIMO Disk Margins

Due to the couplings that exist between the pitch/longitudinal translation loop and the roll/lateral translation loop, stability must also be studied in a MIMO sense. This is done using *multiloop disk margins*, an analysis technique based on the *structured singular value* that can be used to quantify the largest complex perturbations that can be injected at the input point to the plant, simultaneously and independently in each channel (see Fig. 22). The perturbation takes the form of a disk in the complex plane, as illustrated in Fig. 23. Based on the radius of this disk, gain and phase margins can be
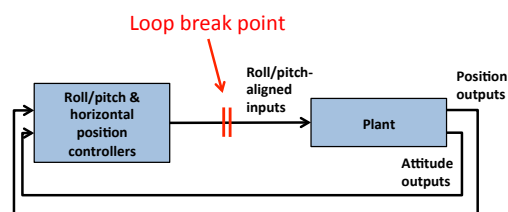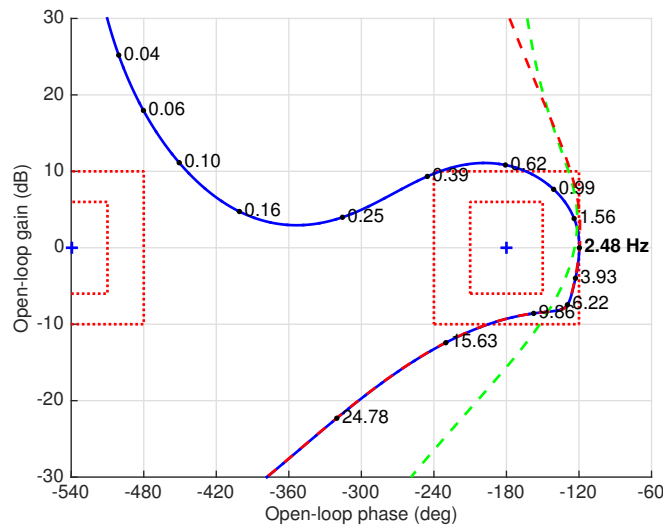
**Fig. 21   Nichols chart for the pitch and longitudinal position control loop, when opened at the input point to the plant (blue, solid). For reference, the inner loop (red, dashed), and outer loop (green, dashed) are also shown.**

computed as indicated in Fig. 23. These margins are inherently conservative relative to classical SISO margins, but have nonetheless proven to be reliable measures of stability margins in the helicopter control design. Several versions of disk margins can be computed, dependent on how perturbations are structured for the purpose of the structured singular value analysis; we use the version described by Blight et al. [28] and implemented by the Matlab *loopmargin* function. For the design presented here, the margins are 8.9 dB and 50 deg.
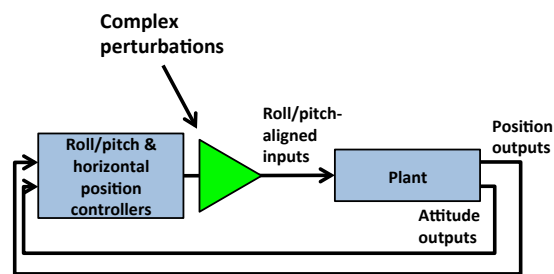


**Fig. 22   Illustration of complex perturbation being injected at a particular place in the control loop. Multiloop disk margins quantify the magnitude of the perturbation that can be tolerated without destabilizing the system.**
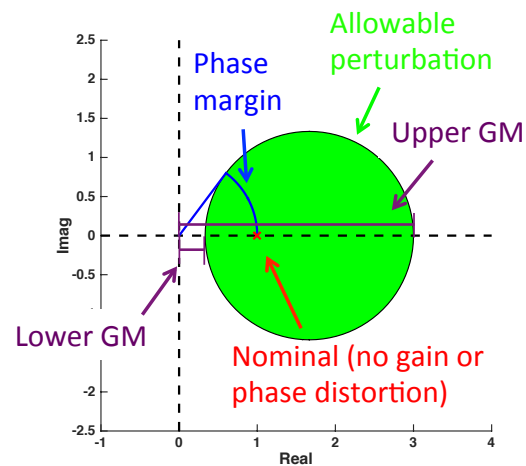


**Fig. 23   Illustration of disk margins and how they relate to notions of gain and phase margins.**

### E. Gust Response

Figure 24 shows the longitudinal position and velocity response to a horizontal gust of magnitude 5 m/s, with a peak displacement of approximately 1.5 m.
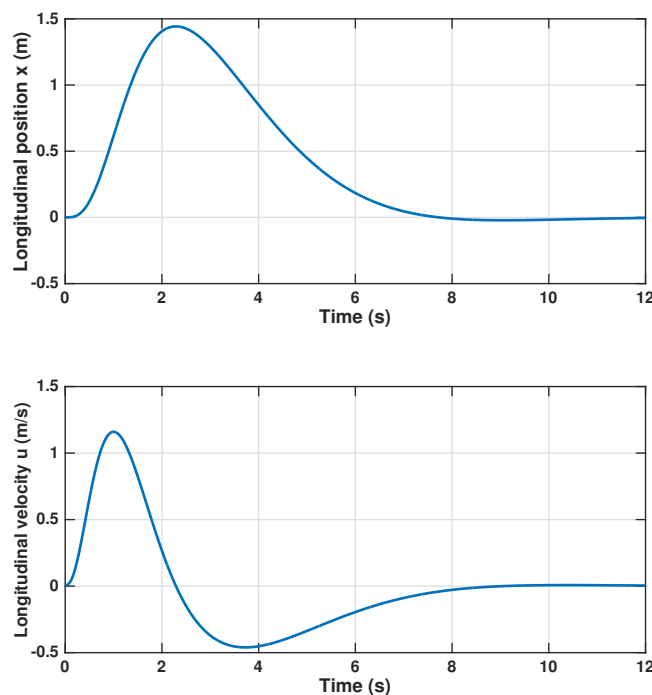
**Fig. 24   Step response of longitudinal position (top plot) and longitudinal velocity (bottom plot) to a gust of magnitude 5 m/s along the *x* axis.**

### F. Notch Filtering of Rotor Harmonics

Notch filters were employed in series with each control input to eliminate the harmonics at 1, 2, 3 and 4 times the frequency of the rotor rotation. This avoids feeding back high-frequency vibrations to the servo actuators, thereby reducing stress on the actuators and helping prevent saturation. The notches are not evident in the Nichols charts shown above, because they occur at higher frequencies, well away from the critical point.

## X. Results of Free-Flight Demonstration

The controller design described in this paper was used to fly the demonstration vehicle in JPL's 25-ft Space Simulator in $CO_2$ at a density of 0.0175 kg/m$^3$. The flight was fully autonomous, consisting of takeoff, climb to an altitude of 2 m at a rate of 1 m/s, hover for 30 s, descent at 0.5 m/s, and landing. A picture of the flying vehicle can be seen in Fig. 25.

Figures 26–28 show the position, attitude, and control inputs for the free-flight demonstration. As discussed in Section III, the air mobilized by the rotor is recirculated within the closed volume of the vacuum chamber, resulting in gusty conditions. This manifests itself as variations in the horizontal position during hover, which are compensated by the control system. The behavior and performance during the free-flight test was as expected, thus validating the end-to-end approach to modeling, system
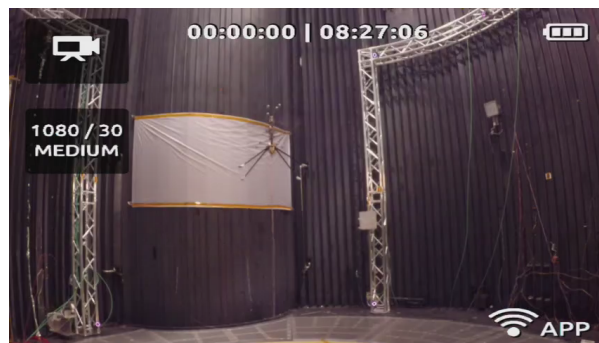


**Fig. 25   The Mars Helicopter demonstration vehicle in hover, inside the JPL 25-ft Space Simulator**

identification, and guidance and control design.

## XI. Concluding Remarks

With the successful free-flight demonstration, the feasibility of controlled helicopter flight on Mars has been established. At the current point in time, development is progressing on a flight-ready Mars vehicle, and tests are being prepared for system identification and flight testing of that vehicle, in addition to environmental tests necessary for Mars flight. A main point of interest in these tests will be the identified vehicle behavior in forward flight, which has been modeled but not covered by actual tests to date. The helicopter dynamics in forward flight tends to exhibit faster instabilities and greater levels of cross-axis coupling, the latter being mitigated by the addition of cyclic on the upper rotor in addition to the lower rotor. Analysis to date shows that adequate stability margins and performance can nonetheless be achieved within the desired flight envelope.
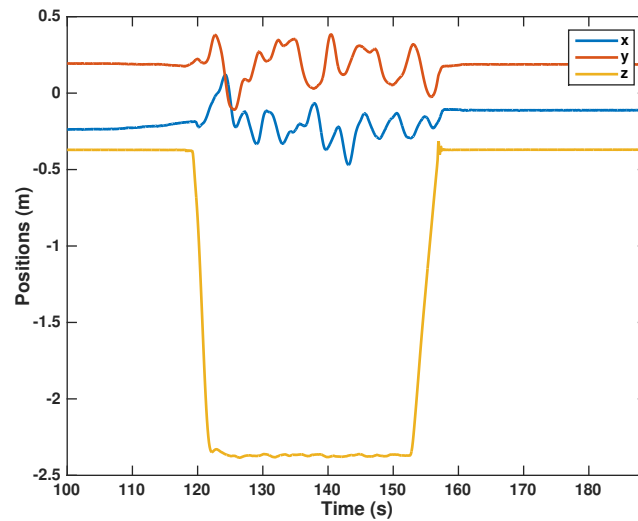


**Fig. 26   Estimated vehicle position (center of mass relative to ground frame, represented in ground frame) during free-flight demonstration. Recall that positive $z$ axis is down.**
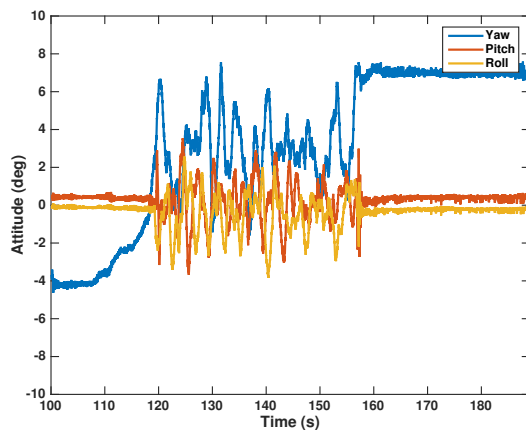


**Fig. 27   Vehicle attitude (body frame relative to ground frame) during free-flight demonstration.**



**Fig. 28   Vehicle control inputs during free-flight demonstration.**

20

## Acknowledgments

## References

[1] Savu, G., and Trifu, O., "Photovoltaic Rotorcraft for Mars Missions," *Proc. Joint Propulsion Conf. and Exhibit*, San Diego, CA, 1995.

[2] Kroo, I., and Kunz, P., "Development of the Mesicopter: A Miniature Autonomous Rotorcraft," *Proc. American Helicopter Society Vertical Lift Aircraft Design Conf.*, San Francisco, CA, 2000.

[3] Aiken, E. W., Ormiston, R. A., and Young, L. A., "Future Directions in Rotorcraft Technology at Ames Research Center," *Proc. American Helicopter Society Annual Forum*, Virginia Beach, VA, 2000.

[4] Young, L. A., "Vertical Lift – Not Just For Terrestrial Flight," *Proc. AHS/AIAA/RaeS/SAE International Powered Lift Conference*, Arlington, VA, 2000.

[5] Young, L. A., et al., "Use of Vertical Lift Planetary Aerial Vehicles for the Exploration of Mars," *NASA Headquarters and Lunar and Planetary Institute Workshop on Mars Exploration Concepts*, Houston, TX, 2000.

[6] Young, L. A., Chen, R. T. N., Aiken, E. W., and Briggs, G. A., "Design Opportunities and Challenges in the Development of Vertical Lift Planetary Aerial Vehicles," *Proc. American Helicopter Society International Vertical Lift Aircraft Design Conference*, San Francisco, CA, 2000.

[7] Thompson, B., "Full Throttle to Mars," Rotor & Wing, Phillips Business Information, LLC, Potomac, MD, 2001.

[8] Datta, A., Roget, B., Griffiths, D., Pugliese, G., Sitaraman, J., Bao, J., Liu, L., and Gamard, O., "Design of the Martian Autonomous Rotary-Wing Vehicle," *Proc. AHS Specialist Meeting on Aerodynamics, Acoustics, and Test and Evaluation*, San Francisco, CA, 2002.

[9] Young, L. A., et al., "Experimental Investigation and Demonstration of Rotary-Wing Technologies for Flight in the Atmosphere of Mars," *Proc. American Helicopter Society Annual Forum Proceedings*, Montreal, Canada, 2002.

[10] Young, L. A., and Aiken, E. W., "Vertical Lift Planetary Aerial Vehicles: Three Planetary Bodies and Four Conceptual Design Cases," *Proc. European Rotorcraft Forum*, Moscow, Russia, 2001.

[11] Young, L. A., et al., "Engineering Studies into Vertical Lift Planetary Aerial Vehicles," *Proc. AHS International Meeting on Advanced Rotorcraft Technology and Life Saving Activities*, Utsunomiya, Tochigi, Japan, 2002.

[12] Young, L. A., Aiken, E. W., Gulick, V., Mancinelli, R., and Briggs, G. A., "Rotorcraft as Mars Scouts," *Proc. IEEE Aerospace Conf.*, Big Sky, MT, 2002.

[13] Young, L. A., Aiken, E. W., and Briggs, G. A., "Smart Rotorcraft Field Assistants for Terrestrial and Planetary Science," *Proc. IEEE Aerospace Conference*, Big Sky, MT, 2004.

[14] Young, L. A., Lee, P., Briggs, G., and Aiken, E., "Mars Rotorcraft: Possibilities, Limitations, and Implications for Human/Robotic Exploration," *Proc. IEEE Aerospace Conference*, Big Sky, MT, 2005.

[15] Tsuzuki, N., Sato, S., and Abe, T., "Conceptual Design and Feasibility for a Miniature Mars Exploration Rotorcraft," *Proc. International Congress of the Aeronautical Sciences*, 2004.

[16] Song, H., and Underwood, C., "A Mars VTOL Aerobot - Preliminary Design, Dynamics and Control," *Proc. IEEE Aerospace Conference*, 2007.

[17] Balaram, J., and Tokumaru, P. T., "Rotorcrafts for Mars Exploration," *Proc. International Planetary Probe Workshop*, Pasadena, CA, 2014. LPI Contribution No. 1795.

[18] Balaram, J., Canham, T., Duncan, C., Golombek, M., Grip, H. F., Maki, J., Quon, A., Stern, R., and Zhu, D., "Mars Helicopter Technology Demonstrator," *Proc. AIAA Atmospheric Flight Mechanics Conference*, 2017.

[19] Grip, H. F., Johnson, W., Malpica, C., Scharf, D. P., Mandić, M., Young, L., Allan, B., Mettler, B., and San Martin, M., "Flight dynamics of a Mars Helicopter," *Proc. European Rotorcraft Forum*, Milan, Italy, 2017.

[20] Mettler, B., *Identification Modeling and Characteristics of Miniature Rotorcraft*, Kluwer Academic Publishers, 2010.

[21] Padfield, G. D., *Helicopter Flight Dynamics: The Theory and Application of Flying Qualitites and Simulation Modeling*, AIAA, 1996.

[22] Lim, C., and Jain, A., "Dshell++: A Component Based, Reusable Space System Simulation Framework," *Proc. Third IEEE International Conference on Space Mission Challenges for Information Technology*, Pasadena, CA, 2009.

[23] Johnson, W., *Rotorcraft Aeromechanics*, Cambridge University Press, 2013.

[24] Peters, D. A., and HaQuang, N., "Dynamic Inflow for Practical Applications," *J. American Helicopter Society*, Vol. 33, No. 4, 1988, pp. 64–68.

[25] Lopez, M., and Prasad, J. V. R., "Linear Time Invariant Approximations of Linear Time Periodic Systems," *Proc. European Rotorcraft Forum*, Munich, Germany, 2015.

[26] Stein, G., "Respect the Unstable," *IEEE Control Systems Magazine*, Vol. 23, No. 4, 2003, pp. 12–25.

[27] Lurie, B. J., and Enright, P. J., *Classical Feedback Control: With Matlab and Simulink*, 2nd ed., CRC Press, 2011.

[28] Blight, J. D., Dailey, R. L., and Gangsaas, D., "Practical control law design for aircraft using multivariable techniques," *Int. J. Control*, Vol. 59, No. 1, 1994, pp. 93–137.